Springer

Journal of Mechanical Science and Technology 22 (2008) 2563~2577

Journal of Mechanical Science and Technology

www.springerlink.com/content/1738-494x
DOI 10.1007/s12206-008-0711-3

Turbulent heat transfer of supercritical carbon dioxide in square cross-sectional duct flow †

Seong Ho Han[1], Young Don Choi[1,*], Jong Keun Shin[2], Young Chan Kim[1] and Min Soo Kim[3]

[1]*Department of Mechanical Engineering, Korea University, Seoul, 136-701, Korea*
[2]*Department of Automotive Engineering, Hanzhong University, 119, Jiheung-dong, Donghae, Kangwondo 240-713, Korea*
[3]*Department of Mechanical Engineering, Seoul National University, Seoul, 151-742, Korea*

(Manuscript Received April 4, 2008; Revised July 14, 2008; Accepted July 16, 2008)

Abstract

Numerical simulations are performed to develop a new heat transfer coefficient correlation applicable to the gas cooler design of a trans-critical carbon dioxide air-conditioner. Thermodynamic and transport properties of the supercritical gas cooling process change dramatically and significantly vary heat transfer coefficients to be much different from those of single or two phase flows. In the present study, the elliptic blending second moment turbulent closure precisely reflecting the effects of these thermo-physical property variations on the turbulent heat transfer is employed to model the Reynolds stresses and turbulent heat fluxes in the momentum and energy equations. Computational results related to the development of turbulent heat transfer during in-duct cooling of supercritical carbon dioxide were used to establish a new heat transfer coefficient correlation that would be widely applicable to a gas cooler design involving turbulent heat transfer of supercritical carbon dioxide in square cross-sectional duct flows.

Keywords: Supercritical state; Carbon dioxide; Heat transfer coefficient correlation; Buoyant generation; Elliptic blending model; Reynolds stress model; Thermal expansion coefficient

1. Introduction

Because CFC and HCFC refrigerants may cause global warming and ozone depletion, the trans-critical carbon dioxide (R-744) cycle has recently received much attention as an alternative refrigerant for air conditioners. Carbon dioxide in trans-critical state possesses high specific heat and excellent thermodynamic and transport properties, making it a good alternative refrigerant. One of the major differences between the trans-critical carbon dioxide cycle and the conventional cycle is the heat rejection process. In the trans-critical cycle, the heat rejection process cools the high pressure carbon dioxide gas along the supercritical isobar. As a result, the thermo-physical properties of the carbon dioxide change drastically, but the phase does not. Therefore, the heat rejection process is called a "gas cooling " process instead of a "condensing" process. Correct prediction of the heat transfer rate in the gas cooling process has been recognized as the most important factor in the design of an efficient air conditioner using the carbon dioxide refrigerant.

Generally, during in-duct cooling of supercritical carbon dioxide under high heat flux conditions, the density ratio between the near wall and core regions of the duct exceeds 3. The production of secondary flow and turbulent kinetic energy induced by the sharp differentiation of density dramatically enhances the heat transfer coefficient of the duct wall.

Various experimental investigations have been performed to obtain the heat transfer coefficient correlation that can be efficiently used for the design of gas

† This paper was recommended for publication in revised form by Associate Editor Kyung-Soo Yang

*Corresponding author. Tel.: +82 2 3290 3355, Fax.: +82 2 928 1067
E-mail address: ydchoi@korea.ac.kr

coolers of the trans-critical carbon dioxide cycle. Petukhov et al. [1], Krasnoshchekov et al. [2], Baskov et al. [3], and Petrov and Popov [4] proposed the heat transfer coefficient correlations for turbulent supercritical carbon dioxide flow. However, their proposed heat transfer coefficient correlations have not be confirmed to be reliable for the design of gas coolers of carbon dioxide air conditioners. There have been difficulties in correctly measuring the heat transfer coefficients from in-tube cooling of supercritical carbon dioxide under high heat flux conditions. As carbon dioxide flow approaches the pseudo-critical point, many parameters such as the pressure, temperature, wall heat flux, Reynolds number and compressibility factor, etc. influence the turbulent heat transfer process from the supercritical carbon dioxide within tubes or ducts.

The heat transfer coefficient can be determined by solving the governing equations of continuity, momentum and energy. In many respects, it is more efficient to obtain the turbulent heat transfer coefficient correlation for the supercritical carbon dioxide in duct cooling or heating by computation than by experiments only. Computation can be performed at remarkable speed at low cost, and computational solution can give detailed and complete information. It can provide the values of all the relevant variables throughout the domain of interest. Moreover, realistic and ideal conditions can be easily and exactly simulated. However, to obtain the available data sufficient for establishing a heat transfer coefficient correlation from the computational results for turbulent supercritical carbon dioxide flows, the turbulence models used in the computation should be validated carefully.

A number of first order turbulence closures employing the eddy diffusivity model have been introduced to predict the turbulent heat transfer of supercritical carbon dioxide flow. A mixing length model developed by Bellmore and Reid [5] has been widely used by various investigators to predict the turbulent heat transfer coefficients of supercritical carbon dioxide flows. Bellmore and Reid [5] used the thermal expansion coefficient (β) to relate the turbulent density fluctuations to the energy fluctuations in the flow field. Pitla et al. [6] abandoned Bellmore and Reid [5] model in favor of a more elegant approach. They obtained a new heat transfer coefficient correlation by curve fitting the numerical data to the experimental data. Comparing the new heat transfer coefficient correlation with three existing correlations, they found that the accuracy of their correlations was much improved.

Although the introduction of the first order turbulence models has much improved the prediction of turbulent heat transfer from supercritical carbon dioxide in tube flow, the first order closures always suffered from the eddy diffusivity concept and could not reflect the effects of buoyancy and drastic change of thermo-physical properties in the vicinity of the pseudo-critical point of heat transfer characteristics.

The buoyant force acting on a fluid affects the turbulence structure by generation and redistribution of the Reynolds stress. As a result, the turbulent heat transfer of supercritical carbon dioxide in duct flow becomes very complex under a high heat flux condition.

In the destabilizing region, a sharp density gradient in the vicinity of the wall generates Reynolds stress while in the stabilizing region it reduces the Reynolds stress. This opposite phenomenon is amplified further the gas flow approaches the pseudo-critical point. Unfortunately, the eddy viscosity model can not appropriately consider the destabilizing and stabilizing effects of buoyancy on the generation and redistribution of the Reynolds stress.

One of the objectives of the present study is to apply the elliptic blending second moment turbulence closure in the analysis of turbulent heat transfer from supercritical carbon dioxide in duct flows.

A number of computations are performed with variations of the wall heat flux and Reynolds number in a horizontal duct with a square cross-section. The computational results for various conditions of wall heat flux and inlet pressure are used to establish a new heat transfer coefficient correlation of supercritical carbon dioxide flow in square cross-sectional ducts for wide application to gas cooler design involving the trans-critical carbon dioxide cycle.

2. Mathematical model

In the present computational work, the square cross-sectional duct is selected in the analysis of the object flow for establishing a new heat transfer coefficient correlation because the cross-sectional shapes of many micro-channels in gas coolers of carbon dioxide air conditioners are close to square.

2.1 Mean flow equations

The three-dimensional equations governing the distribution of the mean velocity components and energy

of compressible and turbulent flows may be expressed as follows

Continuity

$$\frac{\partial}{\partial x_i}\left(\rho U_i\right)=0 \tag{1}$$

Mean Momentum

$$\frac{\partial}{\partial x_j}\left(\rho U_i U_j\right)=-\frac{\partial P}{\partial x_i}+\frac{\partial}{\partial x_j}\left[\mu\left(\frac{\partial U_i}{\partial x_j}+\frac{\partial U_j}{\partial x_i}\right)-\rho\overline{u_i u_j}\right] + g_i\left(\rho_0-\rho\right) \tag{2}$$

Energy

$$\rho U_j\frac{\partial T}{\partial x_j}=\frac{\partial}{\partial x_j}\left(\frac{\mu}{\mathrm{Pr}}\frac{\partial T}{\partial x_j}-\rho\overline{u_j\theta}\right) \tag{3}$$

A second moment turbulence closure is introduced for determining the Reynolds stresses $\overline{u_i u_j}$ appearing in the mean momentum equations, and the turbulent heat fluxes $\overline{u_j\theta}$ in the energy equation. The last term on the right hand side of Eq. (2) is the buoyant force term. As the super-critical carbon dioxide flow in a duct approaches the pseudo – critical point during the gas cooling process, the buoyant force due to the sharp differentiation of the density between the wall and core regions of the duct induces a strong secondary flow that dramatically increases the heat transfer coefficient of the duct wall.

2.2 Turbulence model

2.2.1 Elliptic blending model for the turbulence stress tensor

The model transport equations for the turbulent stress tensor and the energy dissipation rate, which constitute an elliptic blending second-moment closure (Manceau and Hanjalic [7], Manceau [8], Thielen *et al*. [9]), can be given as follows:

$$\frac{D\overline{u_i u_j}}{Dt}=\frac{\partial}{\partial x_k}\left(\left(\nu\delta_{kl}+C_s\overline{u_k u_l}\,\tau\right)\frac{\partial\overline{u_i u_j}}{\partial x_l}\right) +P_{ij}+G_{ij}+\Phi_{ij}^{*}-\varepsilon_{ij} \tag{4}$$

$$\frac{D\varepsilon}{Dt}=\frac{\partial}{\partial x_k}\left(\left(\nu\delta_{kl}+C_\varepsilon\overline{u_k u_l}\,\tau\right)\frac{\partial\varepsilon}{\partial x_l}\right) +C_{\varepsilon 1}\frac{(P_{kk}+G_{kk})}{2\tau}-C_{\varepsilon 2}\frac{\varepsilon}{\tau} \tag{5}$$

where P_{ij} and ε_{ij} are identified as the stress production and dissipation rates, respectively, with $P=P_{kk}/2$ and $\varepsilon=\varepsilon_{kk}/2$, and Φ_{ij}^{*} is the redistribution term. Also, G_{ij} is the generation due to the buoyant effect and can be written as:

$$G_{ij}=-g_i\beta\overline{u_j\theta}-g_j\beta\overline{u_i\theta} \tag{6}$$

where β is the thermal expansion coefficient defined as:

$$\beta=-\frac{1}{\rho}\frac{\partial\rho}{\partial T}\bigg|_P \tag{7}$$

Buoyant force induced by local thermal stratifications in duct flow affects the turbulence structure by both the buoyant generation and redistribution terms in the Reynolds stress and turbulent heat flux equations. The buoyant generation term G_{ij} is proportional to the thermal expansion coefficient β as shown in the Eq. (7).

For an ideal gas, the gas state is represented as $P=\rho RT$, and the thermal expansion coefficient is given by $\beta=1/T$; for an non-ideal gas, however, as the gas state is represented by $P=Z\rho RT$, and the thermal expansion coefficient changes to

$$\beta=\frac{1}{T}+\frac{dZ}{ZdT} \tag{8}$$

where Z is the compressibility factor that illustrates the departure of a pure substance from the ideal – gas behavior.

As the supercritical carbon dioxide flow approaches the pseudo-critical point, the gradient of the compressibility factor increases sharply so that the $\frac{dZ}{ZdT}$ term in the thermal expansion coefficient formulation (8) increases and the ratio of buoyant to shear generations of Reynolds stresses increases sharply. In the present second moment turbulence closure, the effects of the thermal expansion coefficient on the $\overline{u_i u_j}$ and $\overline{u_i\theta}$ equations are considered elaborately through the G_{ij} and $G_{i\theta}$ models.

To impose the limiting wall behavior of the fluctuating quantities of the Reynolds stresses, Manceau [8] proposed the elliptic blending method, which blends the "homogeneous" (away-from the wall) and near-wall models of Φ_{ij}^{*} and ε_{ij} as follows:

$$\Phi_{ij}^{*} = \left(1-\psi^2\right)\Phi_{ij}^{w} + \psi^2\Phi_{ij}^{h} \tag{9}$$

$$\varepsilon_{ij} = \left(1-\psi^2\right)\frac{\overline{u_i u_j}}{k}\varepsilon + \psi^2\left(\frac{2}{3}\varepsilon\delta_{ij}\right) \tag{10}$$

where ψ is an elliptic blending parameter, obtained by solving the elliptic differential equation

$$\psi - L^2\nabla^2\psi = 1, \tag{11}$$

with the boundary condition $\psi = 0$ at the wall. For the reproduction of the wall-limiting behavior of Φ^{w}_{ij}, Manceau and Hanjalic [7] suggested the near-wall redistribution term, and a new unit wall-normal vector formulation as follows.

$$\Phi_{ij}^{w} = -5\frac{\varepsilon}{k}\left(\overline{u_i u_k}\, n_j n_k + \overline{u_j u_k}\, n_i n_k - \frac{1}{2}\overline{u_k u_l}\, n_k n_l\left(n_i n_j + \delta_{ij}\right)\right) \tag{12}$$

$$\mathrm{n} = \frac{\nabla\psi}{\left\|\nabla\psi\right\|} \tag{13}$$

In the quasi-homogeneous model $\Phi_{ij}^{h} = \Phi_{ij}^{slow} + \Phi_{ij}^{rapid}$, Manceau and Hanjalic [7] adopted the following model of Speziale *et al*. [10].

$$\begin{aligned}\Phi_{ij}^{h} = &-\left(C_1 + C_1^{*}\frac{P_{kk}}{2\varepsilon}\right)\varepsilon b_{ij} + C_2\left(b_{ik}b_{kj} - \frac{1}{3}b_{kl}b_{kl}\delta_{ij}\right)\\ &+\left(C_3 - C_3^{*}\sqrt{b_{kl}b_{kl}}\right)k\,S_{ij} + C_4 k\left(b_{ik}S_{jk} + b_{jk}S_{ik} - \frac{2}{3}b_{lm}S_{lm}\delta_{ij}\right)\\ &+C_5 k\left(b_{ik}W_{jk} + b_{jk}W_{ik}\right) - C_{6\theta}\left(G_{ij} - \frac{1}{3}G_{kk}\delta_{ij}\right)\end{aligned} \tag{14}$$

with

$$b_{ij} = \frac{\overline{u_i u_j}}{2k} - \frac{1}{3}\delta_{ij},\quad S_{ij} = \frac{1}{2}\left(\frac{\partial U_i}{\partial x_j} + \frac{\partial U_j}{\partial x_i}\right),$$
$$W_{ij} = \frac{1}{2}\left(\frac{\partial U_i}{\partial x_j} - \frac{\partial U_j}{\partial x_i}\right) \tag{15}$$

The last term of Eq. (14) represents the buoyancy effect, which is considered in the present study but not included in the original model of Speziale et al. [10].

In the above equations, the turbulent time scale τ and length scale L are bounded by Kolmogorov scales as follows (Durbin [11]):

Table 1. The model coefficients for the elliptic blending model.

C_s	C_ε	$C_{\varepsilon 1}^{0}$	$C_{\varepsilon 2}$	C_1	C_1^{*}	C_2	C_3	C_3^{*}	C_4	C_5	$C_{6\theta}$	C_τ	C_L	C_η
0.21	0.18	1.44	1.83	3.4	1.8	0	0.8	1.3	1.25	0.4	1.5	6.0	0.161	80.0

$$\tau = \max\left(\frac{k}{\varepsilon}, C_\tau\left(\frac{\nu}{\varepsilon}\right)^{1/2}\right) \tag{16}$$

$$L = C_L\max\left(\frac{k^{3/2}}{\varepsilon}, C_\eta\frac{\nu^{3/4}}{\varepsilon^{1/4}}\right) \tag{17}$$

In the present study, the model coefficients of the elliptic blending model are adopted from the improved version of Manceau [8] and listed in Table 1. And in Eq. (5), coefficient $C_{\varepsilon 1}$ is described as:

$$C_{\varepsilon 1} = C_{\varepsilon 1}^{o}\left(1 + 0.03\left(1-\psi^2\right)\sqrt{\frac{k}{\overline{u_i u_j}n_i n_j}}\right) \tag{18}$$

2.2.2 Turbulent heat flux model using the elliptic blending equation

A mathematical model of the turbulent scalar transport is required to solve the Reynolds-averaged scalar equation. In second-moment closure, the generation term due to the mean velocity as well as the scalar gradients can be handled exactly, and this feature is one of the most attractive advantages in the prediction of complex flows. The transport equation for turbulent scalar flux in the buoyancy-affected field is given as:

$$\frac{D\overline{u_i\theta}}{Dt} = P_{i\theta} + G_{i\theta} + D_{i\theta}^{v} + D_{i\theta}^{t} + \Phi_{i\theta}^{*} - \varepsilon_{i\theta} \tag{19}$$

From left to right, the terms in Eq. (19) represent the convective transport, production terms of turbulent heat flux, buoyant production, viscous diffusive transport, turbulent diffusive transport, pressure-temperature gradient correlation and molecular dissipation of heat fluxes. The turbulent heat flux production and buoyant production can be respectively written as:

$$P_{i\theta} = -\overline{u_i u_k}\frac{\partial T}{\partial x_k} - \overline{u_k\theta}\frac{\partial U_i}{\partial x_k} \tag{20}$$

$$G_{i\theta} = -g_i\beta\overline{\theta^2} \tag{21}$$

Also, the only unknown correlation in Eq. (21), for which another transport equation must be solved, is the temperature variance $\overline{\theta^2}$. For the transport equation, we adopt the UMIST group's model (Launder [12]), which is constructed in a relatively simple form as:

$$\frac{D\overline{\theta^2}}{Dt} = \frac{\partial}{\partial x_k}\left[\left(\nu\delta_{kl} + C_\theta \overline{u_k u_l}\tau\right)\frac{\partial \overline{\theta^2}}{\partial x_l}\right] + 2P_\theta - 2\varepsilon_\theta \quad (22)$$

where P_θ is production term and maintains the exact form as follows:

$$P_\theta = -\overline{u_i\theta}\frac{\partial T}{\partial x_i} \quad (23)$$

And, ε_θ is the dissipation term and, in the present calculations, the model of Launder [12] is adopted as:

$$\varepsilon_\theta = \frac{1}{2R}\overline{\theta^2}\frac{\varepsilon}{k} \quad (24)$$

with constant time scale ratio *R*.

For the modeling of the unclosed term in Eq. (19), the near-wall behavior of the heat flux equations must be considered. Satisfying the limiting behavior of the models at the wall is one of the basic requirements of near-wall modeling. According to the expression of Lai and So [13], the asymptotic behavior of the various terms in Eq. (19) can be determined, and the balance of Eq. (19) can be taken to define the asymptotic behavior of $\Phi^*_{i\theta}$ model. With these near-wall values, a new turbulent heat flux model can be constructed. Firstly, the turbulent diffusion term in Eq. (19) is modeled by the standard gradient transport hypothesis as:

$$D^t_{i\theta} = \frac{\partial}{\partial x_k}\left(C_\theta \overline{u_k u_l}\tau\frac{\partial \overline{u_i\theta}}{\partial x_l}\right) \quad (25)$$

with the adjustable coefficient C_θ.

The molecular diffusion term $D^v_{i\theta}$ also needs to be modeled. In the present study, the model suggested by Shikazono and Kasagi [14] is adopted for the wall limiting condition as:

$$D^v_{i\theta} = \frac{\partial}{\partial x_k}\left(\frac{(\nu+\alpha)}{2}\frac{\partial \overline{u_i\theta}}{\partial x_k} + n_i n_j \frac{(\nu-\alpha)}{6}\frac{\partial \overline{u_j\theta}}{\partial x_k}\right) \quad (26)$$

In Eq. (26), the n_i means the wall normal unit vector.

The pressure-temperature gradient correlation term $\Phi^*_{i\theta}$ and the dissipation term $\varepsilon_{i\theta}$ are major sink terms and need to be carefully modeled. By following the same approach as for the turbulent stress field, we can express the pressure-temperature gradient correlation term $\Phi^*_{i\theta}$ with the elliptic blending equation.

$$\Phi^*_{i\theta} = \left(1-\psi^2\right)\Phi^w_{i\theta} + \psi^2\Phi^h_{i\theta} \quad (27)$$

In the above model, the ellipticity of the model is preserved by solving an elliptic differential equation for ψ. For $\Phi^h_{i\theta}$, any known quasi-homogeneous model can be adopted and the general linear model is chosen in the present study as:

$$\Phi^h_{i\theta} = -C_{1\theta}\frac{\varepsilon}{k}\overline{u_i\theta} + C_{2\theta}\overline{u_j\theta}\frac{\partial U_i}{\partial x_j} + C_{3\theta}\overline{u_i u_j}\frac{\partial T}{\partial x_j} - C_{4\theta}G_{i\theta} \quad (28)$$

The last term of Eq. (28) represents the buoyancy effect, which is considered in buoyancy-affected flows only. Because the molecular destruction in high Reynolds number flows is significant only close to a solid wall, an expression of $\varepsilon_{i\theta}$ satisfying the above constraints together with $\Phi^h_{i\theta}$ can be proposed as:

$$\varepsilon_{i\theta} = \frac{1}{2}\left(1+\frac{1}{\mathrm{Pr}}\right)\frac{\varepsilon}{k}\overline{u_i\theta} \quad (29)$$

To impose the limiting wall behavior of turbulent heat fluxes, $\Phi^w_{i\theta}$ can be modeled in such a way that it approaches its asymptotic value near the wall.

$$\Phi^w_{i\theta} = -\left[1+\frac{1}{2}\left(1+\frac{1}{\mathrm{Pr}}\right)\right]\frac{\varepsilon}{k}\overline{u_k\theta}\,n_k n_i \quad (30)$$

For the reproduction of the limiting wall behavior of $\Phi^w_{i\theta}$, the unit wall-normal vector is used. However, the use of a wall-normal vector must be avoided, because such a quantity is often not well defined for complex geometries. Therefore, in the present work, a new formulation suggested by Manceau and Hanjalic [7] is adopted. Detailed expressions for the present heat flux model form and the model coefficients can be found in reference of Shin et al [17, 18].

The model coefficients for the present elliptic blending heat flux model are listed in Table 2.

Table 2. The model coefficients for the present elliptic blending heat flux model.

C_θ	$C_{1\theta}$	$C_{2\theta}$	$C_{3\theta}$	$C_{4\theta}$	$C_{6\theta}$	R
0.153	2.5	0.45	0.0	0.33	1.5	1.6

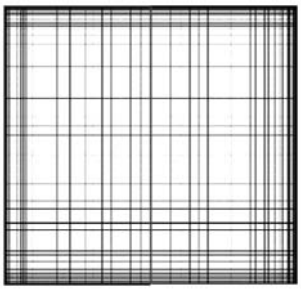

(a)

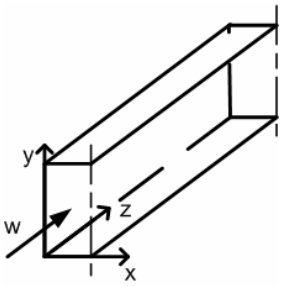

(b)

Fig. 1. Schematic diagram showing a straight duct with a square cross-section.

3. Numerical analysis

3.1 Grid geometry and solving procedure

Fig. 1 illustrates the geometry of the mesh used for the present computational work. The standard grid employed to cover the half cross-section of the duct between the symmetry plane and on each wall was 42 × 80 in the horizontal and vertical directions, respectively, with 16 nodes covering the near-wall sublayer. The first node from the wall was located at $U_2 x_n / \nu < 0.5$ to avoid the use of wall functions. Here x_n is the distance from the (nearest) wall and U_2 is the resultant wall shear velocity at the point on the surface located by dropping a perpendicular from the point in question.

The above-described governing equations are solved using a finite difference forward-marching procedure. The marching is proceeded from an upstream station, where the flow conditions are known, to successive station downstream. The procedure thus computes the flow section by section along the duct length. The usual staggered arrangement of U, V, W and P nodes is adopted, iterated either by way of SIMPLER [15]. The non-diffusive QUICK scheme [16] is used for the discretizing convective transport in the cross-sectional plane of the duct. The mass residual criteria is maintained below 10^{-4} of at each 60000 times iteration until the value is completely converged. Under relaxation factors of energy, momentum, Reynolds stress are set to be 10^{-6}, 10^{-9}, 10^{-9} respectively.

Table 3. Inlet conditions for the present computation.

Re_{in}	P_{in} (MPa)	q (W/m^2)	v_{in} (m/s)	$\dot{m}$ (kg/s)
100,000	7.353	-10,000	1.636	0.0208
		-20,000	1.636	0.0208
		-40,000	1.636	0.0208
	10	-10,000	1.199	0.0226
		-20,000	1.199	0.0226
		-40,000	1.199	0.0226

3.2 Heat transfer of supercritical carbon dioxide flow under high heat flux condition

Turbulent heat transfer of supercritical carbon dioxide in duct flow is much different from normal turbulent heat transfer. The important factor is the secondary flow generated by the drastic change of density in the wall region. During the gas cooling process, more increase in thermal conductivity, specific heat, and density in the wall region than in the core region of the duct may promote the increase of the heat transfer coefficient, but earlier decreases in thermal conductivity, specific heat, and density in the wall region than in the core region of the duct may reduce the heat transfer coefficient during the heating process.

Table 3 shows the inlet and wall heat flux conditions. At the beginning of the computation, duct inlet conditions were specified for the mean velocities U, V, and W, and turbulent kinetic energy k. Fully developed conditions obtained from the precedent calculation were used for the inlet condition. Reynolds stresses at the duct inlet were calculated from the Boussinesq assumption. In all computations, the Reynolds number based on the bulk mean velocity, density, viscosity and hydraulic diameter was fixed to 10^5 at the duct inlet and at the inlet temperature to 373.15 K. Duct inlet pressure was changed to 7.353 MPa and 10 MPa. The isobar of

$P_{in} = 7.353$ MPa passes through the critical point. For each duct inlet pressure, three kinds of heat flux $-10{,}000$ W/m^2, $-20{,}000$ W/m^2 and $-40{,}000$ W/m^2 were applied. The heat transfer computation was continued until the bulk mean temperature of carbon dioxide decreased to about 293.15 K.

3.3 Verification of the present second moment closure

Before the present second moment turbulence closure can be applied to predict the turbulent heat transfer of supercritical carbon dioxide in duct flow under high heat flux condition, which involves a dramatic thermo-physical properties change, the present second moment closure must be verified in the minute heat flux condition.

To verify the present second moment closure, turbulence heat flux was compared with DNS data [17, 18], and turbulence stress of present results was compared with the experimental results [19].

The present heat flux model was validated against available DNS data for various turbulent flows. [17, 18]. Moreover, the predicted distributions of Reynolds stress were compared with the experimental results of the Reynolds stress $\overline{v^2}$ measured by laser doppler velocimeter [19]. In Fig. 2, the present computational results used the elliptic blending model [EBM], and the Reynolds stress model [RSM] used the Shin et al's model [20] and Dol et al's model [21]. The numerical analysis with the same conditions of the occurrence of heat flux on the right and left side wall was conducted at the mass flow rate, $\dot{m} = 0.0127$ kg/s , and heat flux, $q = 80{,}000\,\mathrm{W/m^2}$. The EBM (elliptic blending model) removed of numerical instability in the wall boundary condition coincided with the experimental results in Fig. 2. At $x/D_h = 20$, before fully developed, numerical results disagreed with the experimental results. But at $x/D_h = 80$, the fully developed location, the experimental results coincided with the results of the EBM (elliptic blending model). Especially, the numerical predictions near the wall were more precise with the EBM (elliptic blending model) than with the RSM (Reynolds stress model).

The two Reynolds stress models adopted in the present study involve the wall-reflection term in the pressure-strain model, and the wall-reflection term employs the local distance from the wall. Since the present flow region is directly affected by the four

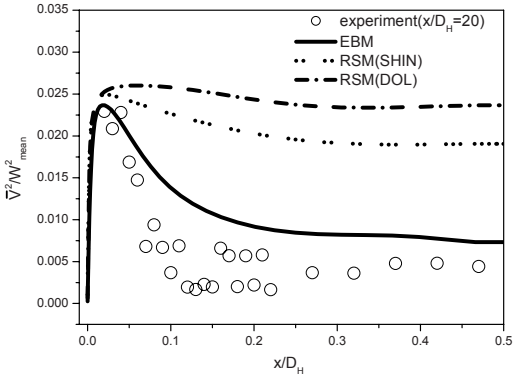

(a)

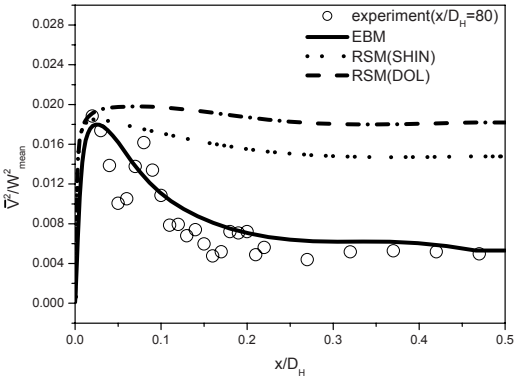

(b)

Fig. 2. Reynolds stress $\overline{v^2}$ distributions at P=7.353 MPa. (a) x/D=20 (b) x/D=80.

walls composing the rectangular duct, we guess that two Reynolds stress models using the wall-reflection term over-predict the profiles of wall-normal direction Reynolds stress. In addition, we can see that the quasi-homogenous part of pressure-strain model adopted in two Reynolds stress models affects on the over-prediction. Although the modifications for the near wall proximity and satisfying the two-component limit are achieved by expressing the model coefficients as functions of invariant turbulence parameters, the quasi-homogeneous models adopted in two Reynolds stress models are directly used to near wall region from the far-from-the-wall homogenous flows without any limitation unlike the elliptic blending model, in which the quasi-homogenous part is controlled by the elliptic blending function as can be seen Eq. (9).

The elliptic blending model removed of the numerical instability in the wall boundary condition

predicted the experimental results more precisely than the Reynolds stress model affected by the wall function. The Reynolds stress model, known to predict inaccurate values near walls, will predict more inaccurate values in the case of super-critical carbon-dioxide flow with sharp change of properties. The distinctive features of turbulence in the region immediately adjacent to a wall are strong inhomogeneity and large anisotropy. Suitable measurement of these near wall turbulence characteristics may be the most important factor for the accurate prediction of turbulent supercritical carbon dioxide flows with wall boundary. Virtually all previous models for the prediction of turbulent supercritical flow of carbon dioxide have used isotropic or quasi-homogeneous assumptions in some significant aspect of their formulations. Such formulations cannot produce Reynolds stresses and turbulent heat fluxes, adequately considering the strong inhomogeneity and large anisotropy in the vicinity of the wall subjected to a large heat flux. Therefore, in all other calculations of this work, we only used the elliptic blending model and the elliptic blending heat flux model.

4. Results and discussion

4.1 Buoyancy effects on the turbulent heat transfer

Turbulent heat transfer of supercritical carbon dioxide flow in a square duct is much different from that of normal state flow because of two reasons. One is the strong secondary flow generated by the sharp density differentiation in the near wall region of the duct. The other is the buoyancy effect generated by density stratification upon turbulence generation in

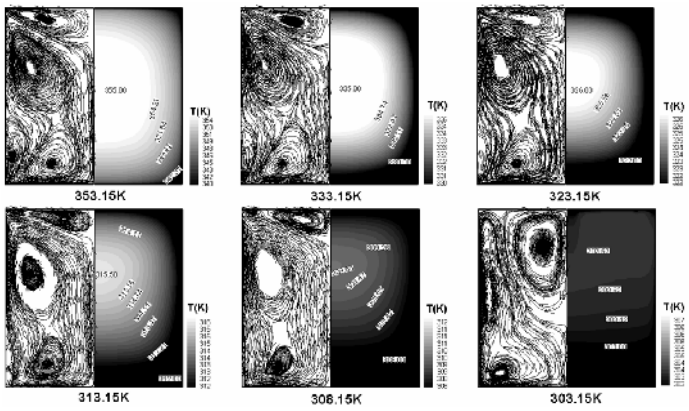

(a)

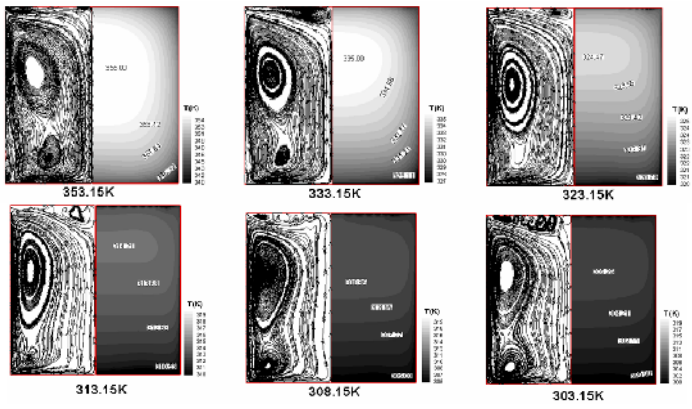

(b)

Fig. 3. Development secondary flow patterns for constant heat flux boundary condition. (a) P_{in} = 7.353 MPa, $q_w = -40,000$ W/m^2 (b) P_{in} = 10 MPa, $q_w = -40,000$ W/m^2 .

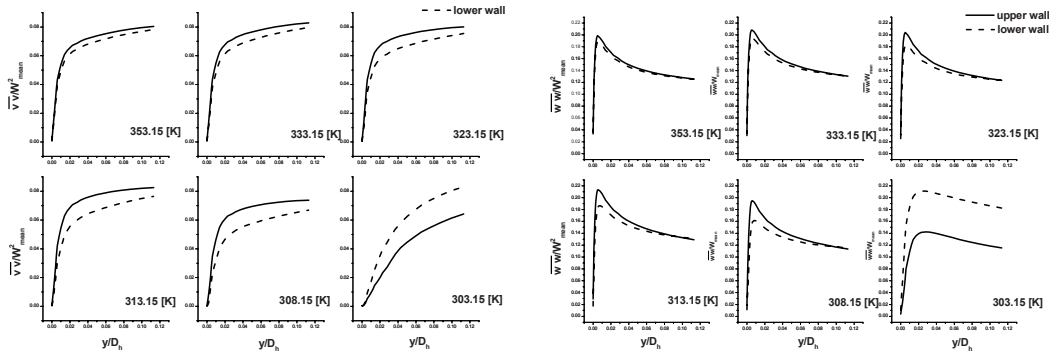

Fig. 4. Development of Reynolds stress profiles for the constant heat flux condition of upper and lower walls for $P_{in} = 7.353$ MPa, $q_w = -40,000$ W/m^2 (a) Reynolds stress $\overline{v^2}$ profiles (a) Reynolds stress $\overline{w^2}$ profiles.

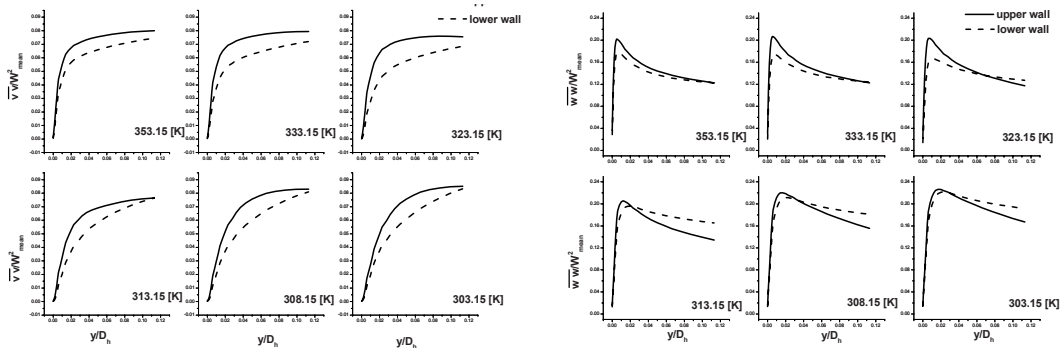

Fig. 5. Development of Reynolds stress profiles for the constant heat flux condition of upper and lower walls for $P_{in} = 10$ MPa, $q_w = -40,000$ W/m^2 (a) Reynolds stress $\overline{v^2}$ profiles (a) Reynolds stress $\overline{w^2}$ profiles.

the near wall region.

During the cooling processes of super-critical carbon dioxide flow in a duct, inhomogeneity of the density between the near wall and core regions generates strong secondary flow motion, as shown in Fig. 3. The secondary flow patterns are greatly changed according to the inlet pressure conditions. In the case of $P_{in} = 10$ MPa condition, the low density fluid generated near the side wall gives rise to strong downward fluid motion, which induces a counter-clockwise vortex flow in the cross-sectional plane of the duct. This counter-clockwise vortex flow enhances the heat transfer of the upper wall region but weakens the heat transfer of the lower wall regions by moving the main stream from lower to upper parts. This moving of the main stream from lower to upper parts steepens the gradients of the streamwise velocity profiles in the upper wall region more than those in the lower wall region. However, in the case of $P_{in} = 7.353$ MPa , T = 303.15 K, properties of carbon dioxide change greatly, and break the secondary flow to form a new flow in the upper wall region, which is different from that of the case where the stable layer is formed in the lower wall region, to reach the critical point in Fig. 3(a), and this new flow can be one reason for the enhancement of the heat transfer in the super-critical state.

Fig. 4 and Fig. 5 show the developments of Reynolds stresses in the upper and lower near wall regions. In the case of $P_{in} = 10$ MPa condition, the Reynolds stress of the upper wall region is always larger than that of the lower wall region, as the cooling process proceeds. In the upper wall region of a horizontal duct, positive buoyant generation destabilizes the flow to enhance the heat transfer but in the lower wall region, negative buoyant generation stabilizes the flow to reduce the heat transfer. Especially, the effect of secondary flow and buoyant turbulence generations promote the heat transfer in the upper region and reduce the heat transfer in the lower wall region.

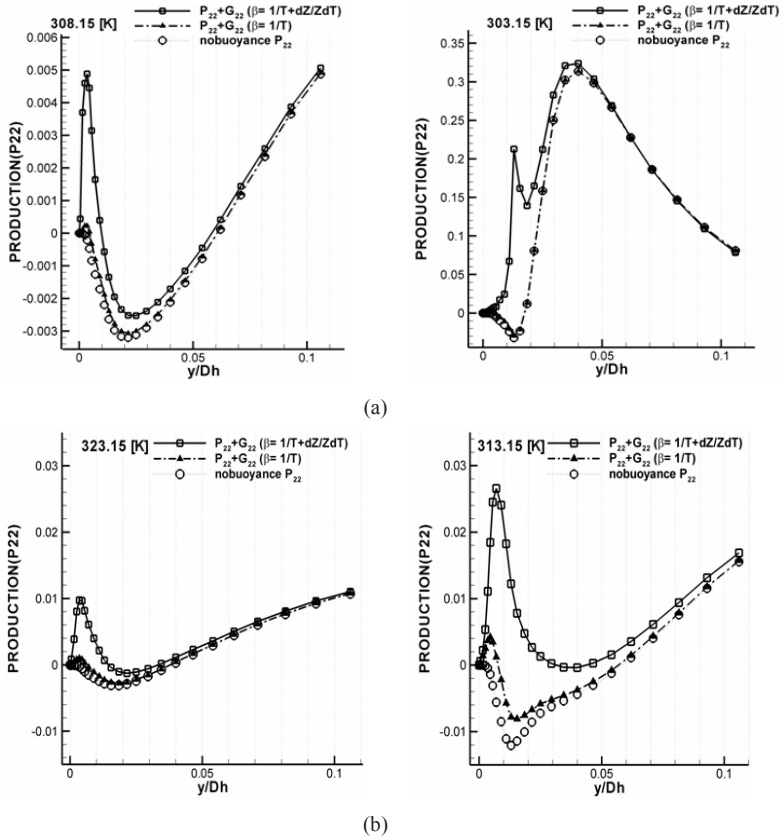

Fig. 6. Development P_{22} of upper wall for $q_w = -40,000\ \mathrm{W/m^2}$ heat flux condition. (a) $P_{in} = 7.353$ MPa (b) $P_{in} = 10$ MPa .

Fig. 6 shows the production term of Eq. (4). The expansion coefficients in Eq. (8), in the cases of $\beta = \frac{1}{T} + \frac{dZ}{ZdT}$, $\beta = \frac{1}{T}$, $\beta = 0$, are compared to each other to consider the effect of the expansion coefficient on the buoyancy production term. This comparison shows that the production term increases steeply in the upper wall region as the carbon-dioxide state reaches the super-critical point. This result is not shown in the case where the buoyancy force and the expansion coefficient are not considered. The increase of the expansion coefficient in the upper wall region causes the buoyancy production term in Eq. (6) to enhance the heat transfer in the upper wall region, as shown in Fig. 6.

4.2 Evaluating of existing turbulent heat transfer coefficient correlation.

Fig. 7 compares experimental results by using Dang el al's experiments [22] with numerical results. This figure shows that the elliptic blending model

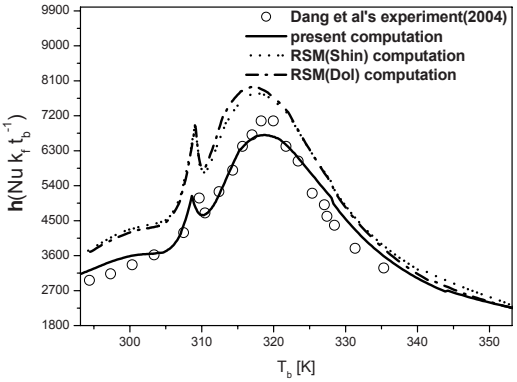

Fig. 7. Comparisons of the heat transfer coefficient predicted by computational results.

obtained in this research showed good agreement with the results of Dang el al's experiments [22]. The results of this research can predict the increase of heat transfer coefficient affected by the property when temperature is between 305.15 K and 313.15 K. At 308 K, which is super-critical point, the property of carbon dioxide varies drastically. At this super-critical

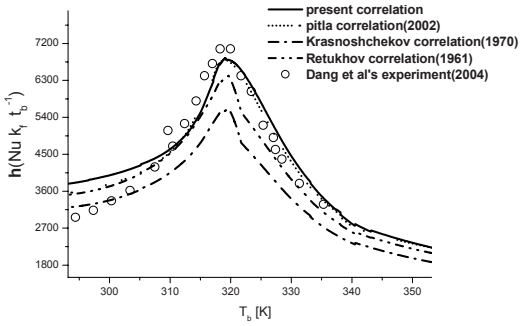

Fig. 8. Comparisons of the heat transfer coefficient predicted by various correlations.

region, density, specific heat, thermal conductivity, viscosity increase rapidly and cause heat transfer to increase. At Fig. 7 and Fig. 8, sharp increase of property creates a cusp nature of heat transfer coefficient near 308K. This phenomenon has been shown in both experiment result and second moment closer model but not in correlation. Also it can be seen from the figure that second moment closure model gave 5-10% higher Nusselt number distribution than that of the present elliptic blending method.

Various correlations based on the results of these investigations have been proposed, and the Nusselt number predicted by existing correlations was compared with the present predictions for the heat cooling process of supercritical carbon dioxide with variation of wall heat flux and duct inlet pressure. On the assumption that the heat transfer coefficient correlation for in-tube supercritical carbon dioxide flow is only little different from that for in-square sectional duct flow, we evaluated the appropriateness of the existing correlations by comparing the results from these existing correlations with the present computational results for the gas cooling process.

The evaluated correlations are as follows.

Retukhov et al's [1] correlation based on the experimental results for the heating of supercritical carbon dioxide in tubes.

$$Nu = Nu_b \left(\frac{\mu_b}{\mu_w}\right)^{0.11} \left(\frac{k_b}{k_w}\right)^{-0.33} \left(\frac{C_{pi}}{C_{pb}}\right)^{0.35} \tag{31}$$

where Nu_b is calculated using the Retukhove Kirillov correlation from Eq. (32).

$$Nu_b = \frac{f/8\ \mathrm{Re}_b \mathrm{Pr}_b}{12.7\sqrt{f/8}\left(\mathrm{Pr}_b^{2/3}-1\right)+1.07} \tag{32}$$

$$f = \frac{1}{\left(0.79\ \ln\ \mathrm{Re}_b - 1.64\right)^2} \tag{33}$$

C_{pi} in correlation (31) is defined as

$$C_{pi} = \frac{i_b - i_w}{T_b - T_w} \tag{34}$$

Krasnoshchekov et al. [2] carried out an experimental study of the heat transfer characteristics during turbulent flow in around a tube with

$$Nu = Nu_b \left(\frac{\rho_b}{\rho_w}\right)^{0.3} \left(\frac{C_{pi}}{C_{pb}}\right)^{n} \tag{35}$$

where,

$$n = 0.4 \quad for \quad T_w/T_{cp} \le 1 \quad or \quad T_b/T_{cp} \ge 1.2$$
$$n = b_1 = 0.22 + 0.18\left(T_w/T_{cp}\right) \quad for \quad 1 \le T_w/T_{cp} < 2.5$$
$$and \quad T_b/T_{cp} \le 1$$
$$n = b_1 + \left(5b_1 - 2\right)\left(1 - T_b/T_{cp}\right) \quad for \quad 1 \le T_w/T_{cp} \le 1.2$$
$$n = 0.7 \quad for \quad T_w/T_{cp} \le 1 \quad and \quad T_w/T_{cp} > 2.5$$

Pitla et al. [6] proposed a new correlation for the Nusselt number based on the numerical prediction. A new correlation was based on the "mean Nusselt number" and was defined as shown in Eq. (36).

$$Nu = \left(\frac{Nu_{wall} + Nu_{bulk}}{2}\right)\frac{k_{wall}}{k_{bulk}} \tag{36}$$

where Nu_w and Nu_b are Nusselt numbers that are evaluated based on the thermophysical properties at the wall and bulk temperatures, respectively. In each case, Grielinski's correlation (37) is used to calculate the respective Nusselt number.

$$Nu = \frac{f/8\left(\mathrm{Re}-1000\right)\mathrm{Pr}}{12.7\sqrt{f/8}\left(\mathrm{Pr}^{2/3}-1\right)+1.07} \tag{37}$$

$$f = \frac{1}{\left(0.79\ln \mathrm{Re} - 1.64\right)^2} \tag{38}$$

All the comparisons were performed for the condition without consideration of the buoyancy-effect. However, the present numerical simulations of supercritical carbon dioxide flow in a square cross sectional duct considered the buoyancy effects on turbulent

heat transfer. We developed a new heat transfer coefficient correlation for supercritical carbon dioxide flow.

Krasnoshchekov and Protopopov [23], Baskov et al. [3], Krasnoshchekov et al. [2] accounted for the effect of the change of thermophysical properties over the cross section of the tube by introducing correction factors for density and specific ratio of the following form.

$$Nu = Nu_b \left(\frac{\rho_w}{\rho_b}\right)^m \left(\frac{C_{pi}}{C_{pb}}\right)^n \tag{39}$$

where Nu_b is calculated using the bulk temperature. But this type of correlation does not consider the effect of free convection. Protopopov et al. [24] characterized the effect of free convection using the ratio of the Grashf and the square of the Reynolds number. For the upward flow in a vertical tube, he proposed the following variation to the correlation given by Eq. (40)

$$Nu = Nu_c \phi(K) \tag{40}$$
$$K = Gr/\mathrm{Re}$$

The value of Nu_c can be calculated by using Eq. (39). In the present numerical analysis, however, we found that in a horizontal duct flow of supercritical carbon dioxide, buoyancy driven secondary flows significantly affected the streamwise velocity distribution and heat transfer characteristics of side walls with the increase of the wall heat flux. Therefore, we proposed the following heat transfer coefficient correlation for cooling of supercritical carbon dioxide in a horizontal square sectional duct.

$$Nu = Nu_b \left(\frac{\rho_w}{\rho_b}\right)^a \left(\frac{C_{pf}}{C_{pb}}\right)^b \left(1 + C\frac{Ri^c}{\mathrm{Pr}^d}\right) \tag{41}$$

We replace C_{pi} in Eq. (39) by C_{pf}, where C_{pf} is the specific heat at the flux temperature $\left(T_f = (T_b + T_w)/2\right)$. The model constructs are found by numerical optimization, and $a = 0.8$, $b = n$, $c = 0.25$, $d = 0.15$ and $C = 0.6$ are adopted, where n is used as the value of Krasnoshchokov et al's [2] correlations:

$$n = 0.4 \quad for \quad T_w/T_{cp} \le 1 \quad or \quad T_b/T_{cp} \ge 1.2,$$
$$n = b_1 = 0.22 + 0.18\left(T_w/T_{cp}\right) \quad for \quad 1 \le T_w/T_{cp} < 2.5 \quad and \quad T_b/T_{cp} \le 1,$$
$$n = b_1 + (5b_1 - 2)\left(1 - T_b/T_{cp}\right) \quad for \quad 1 \le T_w/T_{cp} \le 1.2,$$
$$n = 0.7 \quad for \quad T_w/T_{cp} \le 1 \quad and \quad T_w/T_{cp} > 2.5$$

In Fig. 8, heat transfer coefficient predicted by various correlations is compared with Dang et al's [22] experimental values. The results from the present correlation as well as the Pitla et al's [6] correlation agree with Dang et al's [22] experimental values, but Retukhov et al's [1] and Krasnoshchokov et al's [2] correlations gave somewhat lower values.

Fig. 9 shows the comparisons of Nusselt number predicted by various correlations and the present computational results. The various trends of Nusselt number predicted using the present and Pitla et al's [6]

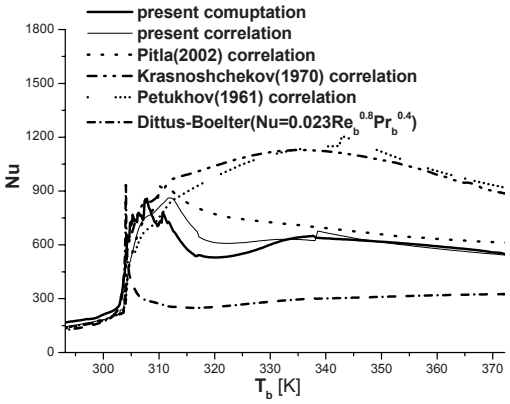

(a)

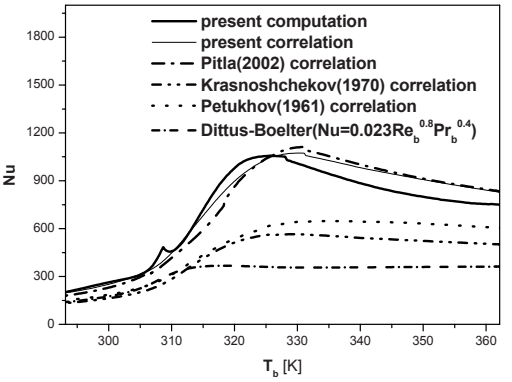

(b)

Fig. 9. Comparisons of Nusselt Number predicted by various correlations. (a) $P_{in} = 7.353$ MPa, $q_w = -40{,}000$ W/m^2 (b) $P_{in} = 10$ MPa, $q_w = -40{,}000$ W/m^2.

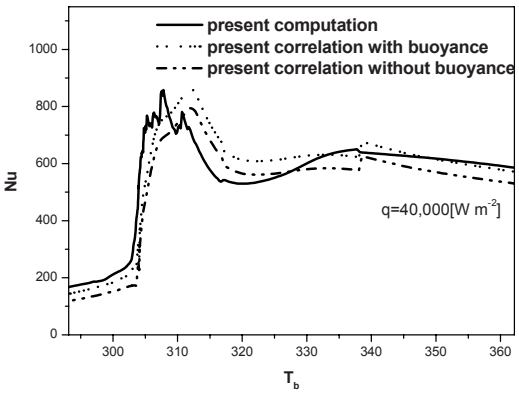

(a)

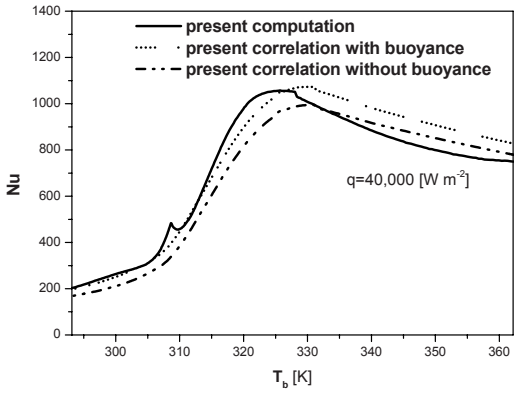

(b)

Fig. 10. Comparisons of present correlation with computational results. (a) $P_{in} = 7.353$ MPa, $q_w = -40,000$ W/m^2 (b) $P_{in} = 10$ MPa, $q_w = -40,000$ W/m^2.

correlation agree most with the present computational results, but at the critical pressure $P_{in} = 7.353$ MPa Pitla et al's [6] correlation show somewhat higher value than the present computational results. At the duct inlet pressure $P_{in} = 10$ MPa, the present correlation and Pitla et al's [6] correlation show very good agreement with the present computational results. Retukhov et al's [1] correlation show the same results as the Krasnoshchokov et al's [2] correlations, except for some differences in the high temperature region. Especially for the critical pressure $P_{in} = 7.353$ MPa, the Nusselt number does not rise with the decrease of the bulk mean temperature, as shown in the computational results. And at the duct inlet pressures $P_{in} = 10$ MPa, Retukhov et al's [1] and Krasnoshchokov et al's [2] correlations give lower values everywhere than the present computational results.

As shown in Fig. 10, the present heat transfer coefficient correlation (41) predicted the Nusselt number for the gas cooling process of supercritical carbon dioxide flow in a square sectional duct. The Nusselt number agreed well with the predictions by numerical analysis for both cases without consideration of buoyancy and with consideration of buoyancy, respectively. The parameter $Ri^{0.25}/\mathrm{Pr}^{0.15}$ is appropriate for reflecting the buoyancy effect on heat transfer in the gas cooling process of supercritical carbon dioxide flow in a square sectional duct. Fig. 10 shows that the present correlation with consideration of buoyance gives Nusselt number distribution that is 5% higher than that without consideration of buoyance. This buoyance effect means the enhancement of turbulence production during heat transfer for a fluid temperature gradient as well as the development of secondary flow through the core region and decrease along the side walls by buoyance.

The various trends of Nusselt number predicted by using the present correlation with consideration of buoyance agree with the present computational result. At $P_{in} = 10$ MPa, the result obtained from the present correlation without consideration of buoyance agrees with the present computational result at high temperatures, but beyond the pseudo-critical temperature, the result obtained from the present correlation with consideration of buoyance agrees with the present computational result.

5. Conclusions

The elliptic-blending second moment closure was applied to the prediction of gas cooling process of turbulent super-critical carbon dioxide flow in a square duct. Computational results showed that a sharp differentiation of density between the near wall and core regions generated strong secondary flow motion. The buoyant generation of turbulence also takes an important role in determining the heat transfer characteristics in the near wall regions.

(1) During the gas cooling process of super-critical carbon dioxide flow, steep increases in density and specific heat of the near wall region were the major cause of the heat transfer enhancement of ducts or pipes.

(2) During the gas cooling process of super-critical carbon dioxide flow, the strong density stratification formed in the vicinity of the wall induced a secondary flow, which increased the heat transfer.

(3) As the super-critical carbon dioxide flow approached the critical or pseudo-critical points, the compressibility factor, which indicates the departure from non-ideality of gas, contributed significantly to the generation and redistribution of the Reynolds stress.

(4) A new heat transfer coefficient correlation was derived from the computational heat transfer of super-critical carbon dioxide flows in a square duct by employing an elliptic-blending moment closure to the Reynolds stress and turbulent heat flux.

Acknowledgment

This work was supported by Korea Science & Engineering Foundation (Grant No R01-2003-000-10571-0)

Nomenclature

b_{ij} : Anisotropic tensor
C_p : Specific heat at constant pressure
D_H : Hydraulic diameter of square cross-sectional duct
g_i : Gravitational acceleration
Gr : Grashf number
h : Heat transfer coefficient
i : Enthalpy
k : Turbulent kinetic energy, heat condu ctivity
$\dot{m}$: Mass flow
n_i : Wall normal vector
Nu : Nusselt number
p : Local pressure
Pr : Prandtl number
q : Heat flux
R : Gas constant
Re : Reynolds number
Ri : Richardson number
S_{ij} : Strain tensor
T : Temperature
u , U : Fluctuating and mean velocity in direction x
$\overline{u_i u_j}$: Kinematic Reynolds stress
$\overline{u_i \theta}$: Turbulent heat flux
v, V : Fluctuating and mean velocity in direction y
w, W : Fluctuating and mean velocity in direction z
W_{ij} : Vorticity tensor
x : Coordinate normal to side wall
y : Coordinate along gravitational direction
z : Coordinate along stream wire direction
Z : Compressibility factor

Greek symbols

α : Thermal diffusivity
β : Thermal expansion coefficient
ε : Dissipation rate of turbulent kinetic energy
ε_{ij} : Dissipation rate of $\overline{u_i u_j}$
$\varepsilon_{i\theta}$: Dissipation rate of $\overline{u_i \theta}$
μ : Dynamic viscosity
ν : Kinematic viscosity
θ : Fluctuating component of temperature
ρ : Density
τ : Turbulent time scale
Φ_{ij} : Pressure strain term of $\overline{u_i u_j}$ equation
$\Phi_{i\theta}$: Pressure scalar gradient term of $\overline{u_i \theta}$ equation

Subscripts

b : Bulk mean
cp : Critical point
in : Inlet
k : Turbulent kinetic energy
m : Mean
θ : Temperature
ε : Dissipation rate of turbulent kinetic energy
t : Turbulence
w : Wall

References

[1] B. S. Petukhov, E. A. Krasnoshchekov and V. S. Protopopov, An Investigation of heat transfer to fluids flowing in pipes under supercritical condition, *ASME International Developments in Heat Transfer,* 3 (1961) 569-578.

[2] E. A. Krasnoshchekov, I. V. Kuraeva and V. S. Protopopov, Local heat transfer of carbon dioxide at supercritical pressure under cooling conditions, *Teplofizika Vysokikh Temperature,* 7 (5) (1970) 922-930.

[3] V. L. Baskov, I. V. Kuraeva and V. S. Protopopov, Heat transfer with the turbulence flow of a liquid at supercritical pressure in tubes under cooling conditions, *Teplofizika Vysokikh Temperature,* 16 (1) (1997) 96-102.

[4] N. E. Petrov and V. N. Propov, Heat transfer and

resistance of carbon dioxide being cooled in the supercritical region, *Thermal Engineering,* 32 (3) (1985) 131-134.

[5] C. P. Bellmore and R. L. Reid, Numerical prediction of wall temperatures for near-critical para-hydrogen in turbulent upflow inside vertical tubes, *Transactions of the ASME,* 105 (3) (1983) 536–541.

[6] S. S. Pitla, E. A. Groll and S. Ramadhyani, New correlation to predict the heat transfer coefficient during in-tube cooling of turbulent supercritical CO2, *Int. J. Refrigeration,* 22 (3) (2002) 887-895.

[7] R. Manceau, An improved version of the elliptic blending model. Application to non-rotating and rotating channel flows, *Proc. 4th Int. Symp. Turb. Shear Flow Phenomena*, Williamsburg, VA, USA, (2005).

[8] R. Manceau and K, Hanjalic, Elliptic blending model: a new near-wall Reynolds-stress turbulence closure, *Phys. Fluids,* 14 (2) (2002) 744-754.

[9] L. Thielen, K. Hanjalic, H. Jonker and R. Manceau, Predictions of flow and heat transfer in multiple impinging jets with an elliptic-blending second-moment closure, *Int. J. Heat mass Transfer,* 48 (8) (2005) 1583-1598.

[10] C. G. Speziale, S. Sarkar and T. B. Gatski, Modeling of the pressure-strain correlation tensor: an invariant dynamical systems approach, *J. Fluid Mech.,* 227 (1991) 245-272.

[11] P. A. Durbin, A Reynolds stress model for near-wall turbulence, *J. Fluid Mech.,* 249 (1993) 465-498.

[12] B. E. Launder, On the computation of convective heat transfer in complex turbulent flow, *J. Heat Transfer,* 110 (1988) 1112-1128.

[13] Y. G. Lai and R. M. C. So, Near-wall modeling of turbulent heat fluxes, *Int. J. Heat Mass Transfer,* 33 (7) (1990) 1429-1440.

[14] N. Shikazono and N. Kasagi, Second-moment closure for turbulent scalar transport at various Prandtl numbers, *Int. J. Heat Mass Transfer,* 39 (14) (1996) 2977-2987.

[15] S. V. Patankar and D. B. Spalding, A calculation procedure for heat, mass and momentum transfer in three dimensional parabolic flow, *Int. J. Heat Mass Transfer,* 15 (10) (1972) 1787-1806.

[16] B. P. Leonard, A stable and accurate convective modeling procedure based on quadratic upstream interpolation, *Computer methods in Applied Mechanics and Engineering,* 19 (1) (1979) 59-98.

[17] J. K. Shin, J. S. An, Y. D. Choi, Y. C. Kim and M. S. Kim, Elliptic Relaxation Second Moment Closure for the Turbulent Heat Fluxes, *J. Turbulence,* 9 (3) (2008) 1-29.

[18] J. K. Shin, J. S. An and Y. D. Choi, Numerical analysis of turbulent flow and heat transfer in a square sectioned u-bend duct by elliptic-blending second moment closure, *J. Mechanical Science and Technology*, 21 (2) (2007) 360-371.

[19] S. H. Han, Y. D. Choi, J. S. Seo, Y. C. Kim and M. S. Kim, Experimental study on the secondary flow characteristics of a supercritical carbon dioxide flow in a gas cooling process within a square duct, *Trans. of the KSME (B),* 32 (2) (2008) 158-165.

[20] J. K. Shin and Y. D. Choi, Development of Low Reynolds Number Second Moment Turbulence Closure by DNS data, *Trans. of the KSME (B),* 20 (8) (1996) 2572-2592.

[21] H. S. Dol, K. Hanjalic and T. A. M. Versteegh, A DNS-based thermal second-moment closure for buoyant convection at vertical walls, *J. Fluid Mech.,* 391 (1999) 211-247.

[22] C. Dang and E. Hihara, In-tube cooling heat transfer of supercritical carbon dioxide. Part 1. Experimental measurement, *Int. J. Refrigeration,* 27 (7) (2004) 736-747.

[23] E. A. Krasnoshchekov and V. S. Protopopov, A generalized relationship for calculation of heat transfer carbon dioxide and supercritical pressure, *Teplofizika Vysokikh Temperature,* 9 (6) (1972) 1314-1320.

[24] V. S. Protopopov, I. V. Kuraeva, T. Peisyue, Diffusion mass transfer with laminar thermogravitational convection of water about a vertical heated wall, *Thermal engineering,* 39 (5) (1992) 260-264.

Seong Ho, Han received a B.S. degree in Mechanical Engineering from Kookmin University in 2003. He then went on to receive his M.S. degree from Korea University in 2005. He is currently in a Ph. D. course at Mechanical Engineering at Korea University in Seoul, Korea. His research interests are in the area of hydrogen energy, polymer electrolyte membrane fuel cell.